

## Research



**Cite this article:** Asadzadeh SS, Nielsen LT, Andersen A, Dölger J, Kjørboe T, Larsen PS, Walther JH. 2019 Hydrodynamic functionality of the lorica in choanoflagellates. *J. R. Soc. Interface* **16**: 20180478.  
<http://dx.doi.org/10.1098/rsif.2018.0478>

Received: 26 June 2018  
 Accepted: 22 November 2018

**Subject Category:**  
 Life Sciences – Physics interface

**Subject Areas:**  
 computational biology

**Keywords:**  
 choanoflagellates, lorica, low Reynolds number flow, computational fluid dynamics, microswimmers, filter feeders

**Author for correspondence:**  
 Jens H. Walther  
 e-mail: [jhw@mek.dtu.dk](mailto:jhw@mek.dtu.dk)

Electronic supplementary material is available online at <https://dx.doi.org/10.6084/m9.figshare.c.4358504>.

# Hydrodynamic functionality of the lorica in choanoflagellates

Seyed Saeed Asadzadeh<sup>1</sup>, Lasse Tor Nielsen<sup>2</sup>, Anders Andersen<sup>3</sup>, Julia Dölger<sup>3</sup>, Thomas Kjørboe<sup>2</sup>, Poul S. Larsen<sup>1</sup> and Jens H. Walther<sup>1,4</sup>

<sup>1</sup>Department of Mechanical Engineering, <sup>2</sup>National Institute of Aquatic Resources and Centre for Ocean Life, and <sup>3</sup>Department of Physics and Centre for Ocean Life, Technical University of Denmark, 2800 Kongens Lyngby, Denmark

<sup>4</sup>Computational Science and Engineering Laboratory, ETH, Zürich, Switzerland

LTN, 0000-0003-4177-3205; AA, 0000-0002-3831-1707; JHW, 0000-0001-8100-9178

Choanoflagellates are unicellular eukaryotes that are ubiquitous in aquatic habitats. They have a single flagellum that creates a flow toward a collar filter composed of filter strands that extend from the cell. In one common group, the loricate choanoflagellates, the cell is suspended in an elaborate basket-like structure, the lorica, the function of which remains unknown. Here, we use Computational Fluid Dynamics to explore the possible hydrodynamic function of the lorica. We use the choanoflagellate *Diaphanoeca grandis* as a model organism. It has been hypothesized that the function of the lorica is to prevent refiltration (flow recirculation) and to increase the drag and, hence, increase the feeding rate and reduce the swimming speed. We find no support for these hypotheses. On the contrary, motile prey are encountered at a much lower rate by the loricate organism. The presence of the lorica does not affect the average swimming speed, but it suppresses the lateral motion and rotation of the cell. Without the lorica, the cell jiggles from side to side while swimming. The unsteady flow generated by the beating flagellum causes reversed flow through the collar filter that may wash away captured prey while it is being transported to the cell body for engulfment. The lorica substantially decreases such flow, hence it potentially increases the capture efficiency. This may be the main adaptive value of the lorica.

## 1. Introduction

Choanoflagellates are filter feeders and an important component of microbial foodwebs [1–3]. They share ancestry with animals and have remarkably common characteristics with the choanocytes of sponges [4]. During the past century, choanoflagellates have been the subject of numerous studies with the goal of understanding the evolution of multicellularity in animals [5,6]. Like other microswimmers, choanoflagellates live in a low Reynolds number world that is dominated by friction and very different from the inertia-dominated world of macroswimmers [7,8]. This is important to these purely heterotrophic organisms that rely exclusively on prey captured from a very dilute suspension, requiring them to daily clear a volume of water corresponding to one million times their own body volume [9].

Choanoflagellates are equipped with a single flagellum that creates a flow toward the collar filter where bacteria-sized prey are retained on the microvilli tentacles. Some choanoflagellates (over 150 species) construct a very ornate extra-cellular basket-like structure, known as the lorica [3] (figure 1). We shall focus on the loricate choanoflagellate *Diaphanoeca grandis* that has a flagellum beating in a plane and a collar filter consisting of approximately 50 microvilli. The lorica of *D. grandis* contains 12 longitudinal and four transverse costae (ribs) [3] (electronic supplementary material, figure S1B). The upper part of the lorica is covered by an organic investment composed of numerous filaments (veil) woven tightly. As the flagellum beats, water enters the lorica chamber from the large spacings between the ribs in the lower part. The water is

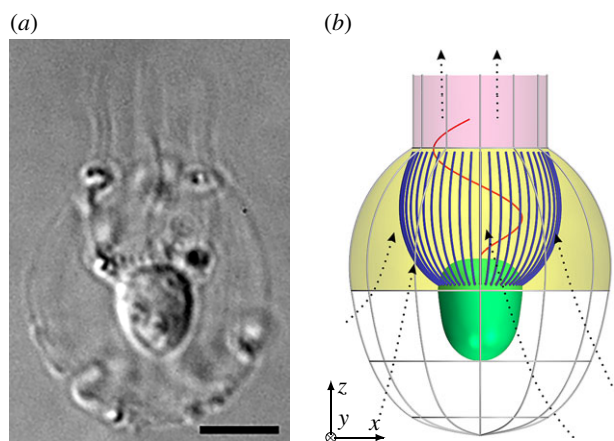


**Figure 1.** Morphology of *Diaphanoeca grandis*. (a) Microscopic image (scale bar, 5  $\mu\text{m}$ ). (b) Model morphology with collar filter composed of 50 microvilli (blue), cell (green), flagellum (red) and lorica containing 12 longitudinal and four transverse ribs (grey) with a fine network of filaments (the veil) on the lorica dome (yellow) and chimney (pink). The arrows indicate the direction of the flow. (Online version in colour.)

transported toward the equator and then passes through the collar filter and finally exits from the chimney. Nielsen *et al.* [6] demonstrated that the observed high flow rate through the collar filter of *D. grandis* can be explained by the inclusion of a flagellar vane, a structure that has been reported in closely related organisms [4,10–13], but has not so far been observed in *D. grandis*. In the choanocytes of the leucon sponge, Asadzadeh *et al.* [14] demonstrated that the presence of the vane together with its interaction with the fine-meshed collar are indispensable for providing sufficiently high pressure to drive the flow through the sponge canal system [15–17].

The presence of the lorica has puzzled scientists for almost a century, and despite extensive research on the morphology, construction and assembly of the lorica, there are only few and limited studies on its functionality [3]. Proposed functionalities are based on pure conjecture by analysing morphological and ecological information [3]. Thus far three functions of the lorica have been proposed: first, the lorica functions as a drag-anchor that counteracts propulsion such that the force generated by the flagellum is rather spent on forcing water through the collar filter [18]. Second, the presence of the fine-meshed veil on the lorica acts in a hydrodynamic sense by funnelling the inflow through the lorica and increases the water flow [18]. Third, the silicified lorica likely reduces the sinking velocity, especially in those species that possess spines [3], analogous to the function of spines in many diatom species [19].

Although the above suggestions seem plausible, they lack evidence and remain speculative. To examine the actual effect of the lorica, one direct approach is to study a loricate species with and without its lorica. However, as pointed out by Pettitt *et al.* [20] this is not a feasible experiment. Here we choose an alternative approach and use computational fluid dynamics (CFD) to study the flow around a single but representative model organism (*D. grandis*) with and without its lorica to elucidate the hydrodynamic functions of the lorica and test the validity of the proposed functionalities. Additionally, we experimentally measured the forward swimming speed of freely swimming individuals of *D. grandis*, and we used the results to validate our CFD simulations.

We first investigate the permeability of the veil on the lorica in a tethered *D. grandis*, and we find that it is practically

impermeable to the flow. Modelling the lorica as an impermeable structure in the upper part, we then study the effect of the lorica on the cell motion and power consumption by the flagellum. We further study the flow rate, the flow recirculation and the resulting clearance rate for the capture of motile and non-motile prey in the freely swimming choanoflagellate. In most cases, the lorica has no beneficial role except in stabilizing cell motion. However, stabilized cell motion reduces the ‘back-flow’ through the filter and thus may increase the efficiency of prey retention on the collar filter.

## 2. Material and methods

In this section, we explain the numerical approach and the method employed for simulating a permeable lorica. We further explain the technique developed to simulate the freely swimming organism as well as our procedure to simulate advective and diffusive prey capture. Finally, we describe the experimental measurements of the swimming speed of *D. grandis*.

### 2.1. Computational fluid dynamics

We use computational fluid dynamics (CFD) simulations to study the flow around *D. grandis*. The domain is discretized by polyhedral cells and a finite volume method is used to discretize and solve the governing equations on each cell by applying the commercial CFD program STAR-CCM+ (12.02.010-R8).

#### 2.1.1. Governing equations and power expenditure

The governing equations of an incompressible Newtonian fluid with density  $\rho$  and viscosity  $\mu$  are the continuity and Navier–Stokes equations

$$\nabla \cdot \mathbf{u} = 0 \quad (2.1)$$

and

$$\rho \left( \frac{\partial \mathbf{u}}{\partial t} + (\mathbf{u} \cdot \nabla) \mathbf{u} \right) = -\nabla p + \mu \nabla^2 \mathbf{u}, \quad (2.2)$$

where  $\mathbf{u}$  and  $p$  denote flow velocity and pressure, respectively.

Figure 2 shows the CFD model of *D. grandis* with applied boundary conditions. Since the observed flow is only obtained by inclusion of a vane on the flagellum and not by a naked flagellum, we model this structure by a 5  $\mu\text{m}$ -wide sheet which beats in a plane [6]. We model the lateral displacement of the flagellum during its beat with the following travelling wave form:

$$d(z, t) = A[1 - e^{-(z-z_B)/\delta}] \sin(k(z - z_B) - \omega t), \quad (2.3)$$

for  $z \geq z_B$  where  $z_B$  is the  $z$ -coordinate of the flagellum at its base on the cell,  $\delta = 1.0 \mu\text{m}$  the characteristic length scale of the amplitude modulation,  $k = 2\pi/\lambda$  the wave number, and  $\omega = 2\pi f$  the angular frequency. The exponential term ensures that the velocity of the flagellum is zero at its base. Table 1 lists the characteristic parameters of the flagellum [6]. The details of the CFD model morphology for cell, filter and lorica are provided in the electronic supplementary material, Section). The Reynolds number is the ratio of inertial to viscous forces, and in small-scale flows around flagellate cells it is much smaller than unity, ranging from  $10^{-2}$  to  $10^{-4}$  [21,22]. Employing  $\rho = 997 \text{ kg m}^{-3}$  and  $\mu = 0.001 \text{ Pa} \cdot \text{s}$ , here  $\text{Re} = \rho L^2 f / \mu \sim 5 \times 10^{-4}$ . Therefore, the inertial terms on the left-hand side of equation (2.2) are negligible and the governing equations reduce to the Stokes equations that are time independent [8]. Hence, it suffices to solve the flow around the choanoflagellate at only some discrete positions of the periodically beating flagellum during a half period. However, here we solve the full Navier–Stokes equations including the unsteady and the nonlinear inertial terms that are both embedded in the STAR-CCM+ software. By retaining the unsteady term and using mesh morphing, which

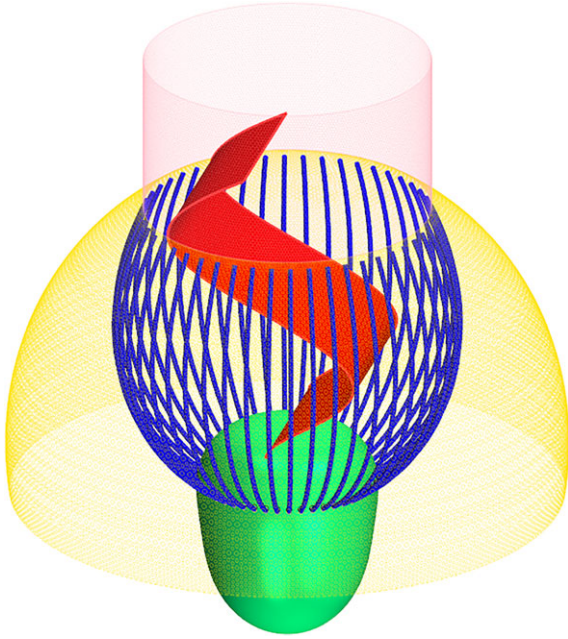


**Figure 2.** CFD model morphology of *Diaphanoeca grandis* with a 5  $\mu\text{m}$  wide flagellar vane (red), the microvilli (blue) and the cell (green) which are all subject to no-slip boundary conditions, and the loricula dome (yellow) and the chimney (pink) treated as porous baffle with adjustable porosity. The ribs in the lower part of the loricula are neglected in the CFD model. (Online version in colour.)

**Table 1.** Characteristic parameters of the flagellum in *D. grandis* [6].  $A$  is the amplitude,  $L$  the length on the central  $z$ -axis,  $f$  the frequency,  $\lambda$  the wavelength and  $W$  the width of the flagellar vane.

| $A$ ( $\mu\text{m}$ ) | $L$ ( $\mu\text{m}$ ) | $f$ (Hz) | $\lambda$ ( $\mu\text{m}$ ) | $W$ ( $\mu\text{m}$ ) |
|-----------------------|-----------------------|----------|-----------------------------|-----------------------|
| 2.8                   | 8.3                   | 7.3      | 8.6                         | 5                     |

redistributes mesh vertices in response to the movement of the flagellum, the new position of the flagellum is updated during each time step. This method dramatically reduces the extra work of otherwise constructing the new geometry and repeated generation of the finite volume mesh.

The flagellar vane, the microvilli and the cell are subject to the no-slip boundary condition. The loricula in the upper part is treated as a permeable surface with adjustable porosity to study the effect of the loricula pore size on the flow, but as an impermeable surface in the remainder of this study. The ribs in the lower part are neglected in the CFD simulations. The whole organism is inserted inside a spherical domain, and a pressure boundary condition is applied on the external boundary. The computational domain is discretized with 4.8 and 2.3 million computational cells for loriculate and non-loriculate cases, respectively. In both cases, the force and the flow rate are independent of the number of cells (approx. 2% variations). For the advection and diffusion problem, the mesh is further refined on and in between the microvilli and downstream of the collar, where the concentration gradients are high, resulting in 12 and 13 million computational cells for loriculate and non-loriculate cases, respectively. Finally, to ensure independence of the size of the domain, we solve the governing equations on three different domain sizes with diameters of 60  $\mu\text{m}$ , 80  $\mu\text{m}$  and 120  $\mu\text{m}$ , and we find less than 1% variations in the results. Therefore, we use a domain with a diameter of 60  $\mu\text{m}$ .

Once the velocity field has been determined, the power ( $P$ ) expended by the beating flagellum is calculated as the surface integral over the flagellum area ( $S_{fl}$ ) of its local velocity (equation (2.3)) times the resultant stress vector ( $\sigma \cdot \mathbf{n}$ ). We verify that the

total power expenditure equals the volume integral over the fluid domain ( $V$ ) of the viscous dissipation:

$$P = \iint_{S_{fl}} \mathbf{u} \cdot (\sigma \cdot \mathbf{n}) dS = 2\mu \iiint_V \mathbf{E} : \mathbf{E} dV, \quad (2.4)$$

where  $\mathbf{n}$  denotes the unit normal vector on the surface  $S_{fl}$  pointing into the fluid and  $\mathbf{E} = (\nabla \mathbf{u} + (\nabla \mathbf{u})^T)/2$  the fluid strain rate tensor [23]. Equation (2.4) is valid for both tethered and freely swimming organisms.

### 2.1.2. Model of the loricula as a permeable structure

The veil in the upper part of the loricula is composed of approximately 0.01  $\mu\text{m}$  thick filaments with radius  $a = 0.005 \mu\text{m}$ , and it has a pore size  $h = 0.05\text{--}0.5 \mu\text{m}$  [18]. To study the effect of the porosity of the loricula on the flow around the cell, we consider the loricula as a porous baffle that the flow can pass through subject to a pressure drop. We model this structure as a square network of cylinders of spacing  $h$ . The pressure drop ( $\Delta p_p$ ) due to fluid flow through such a network can be related to the velocity normal to the network surface ( $v_n$ ) as

$$\Delta p_p = \frac{16\pi\mu}{h\Lambda_e} v_n, \quad (2.5)$$

where  $\Lambda_e = 1 - 2 \ln \tau + \tau^2/6 - \tau^4/144 + \tau^6/1080 + \dots$  and  $\tau = 2\sqrt{2}\pi a/h$  [24]. Equations (2.1) and (2.2) subject to equation (2.5) are solved to obtain the velocity and pressure fields.

### 2.1.3. Solution procedure to model free swimming

For swimming at low Reynolds numbers, the change in the momentum is negligible compared to the pressure and viscous forces. Therefore, at any instant of time, the forces ( $\mathbf{F}$ ) and torques ( $\mathbf{L}$ ) of the fluid (as given by viscous and pressure forces in the stress tensor) are balanced by any external forces and torques acting on the swimmer [8]:

$$\begin{pmatrix} \mathbf{F} \\ \mathbf{L} \end{pmatrix}_{\text{ext}} + \begin{pmatrix} \mathbf{F} \\ \mathbf{L} \end{pmatrix}_{\text{fluid}} = 0. \quad (2.6)$$

The fluid forces and torques are calculated by integrating the stress tensor over the surface of the swimmer:

$$\mathbf{F} = \iint_S \sigma \cdot \mathbf{n} dS \quad \text{and} \quad \mathbf{L} = \iint_S \mathbf{r} \times (\sigma \cdot \mathbf{n}) dS, \quad (2.7)$$

where  $\mathbf{r}$  denotes the position on the surface  $S$ .

The motion of a microswimmer is a superposition of a deformation and rigid body motion. The rigid body forces and torques are related to the translation velocity and rotation rate through the resistive matrix  $\mathbf{R}$  of the body [8]. In our case, the flagellum beats in the  $xz$ -plane and because of the mirror symmetry with respect to this plane, only translation and rotation in the  $xz$ -plane are allowed. Therefore

$$\mathbf{F}_{\text{ext}} + \mathbf{F}_{\text{def}} + \mathbf{R}\mathbf{U} = 0, \quad (2.8)$$

where

$$\mathbf{F}_{\text{ext}} = \begin{bmatrix} F_x \\ F_z \\ L_y \end{bmatrix}_{\text{ext}}, \quad \mathbf{F}_{\text{def}} = \begin{bmatrix} F_x \\ F_z \\ L_y \end{bmatrix}_{\text{def}}, \quad \mathbf{U} = \begin{bmatrix} U_x \\ U_z \\ \Omega_y \end{bmatrix}$$

Here  $F_x$  and  $F_z$  denote the  $x$  and  $z$  component of the force, and  $U_x$  and  $U_z$  are the  $x$  and  $z$  component of the velocity, respectively.  $L_y$  and  $\Omega_y$  are the torque and rotation rate with respect to an arbitrary point. Here, we choose the base of the flagellum  $(0, 0, z_B)$  as the point about which the organism rotates. The resistive matrix  $\mathbf{R}$  is a square  $3 \times 3$  matrix:

$$\mathbf{R} = \begin{bmatrix} r_{11} & r_{12} & r_{13} \\ r_{21} & r_{22} & r_{23} \\ r_{31} & r_{32} & r_{33} \end{bmatrix}.$$

The unknown matrix elements depend on the shape of the organism and since the flagellum is constantly changing its shape, the matrix is also time-dependent. It can be shown that  $\mathbf{R}$  is always symmetric, resulting in six unknowns in the matrix [25]. In the absence of any external forces and torque, the organism is freely swimming and equation (2.8) reduces to

$$\mathbf{F}_{\text{def}} + \mathbf{R}\hat{\mathbf{U}} = 0, \quad (2.9)$$

where

$$\hat{\mathbf{U}} = \begin{bmatrix} \hat{U}_x \\ \hat{U}_z \\ \hat{\Omega}_y \end{bmatrix}$$

represents the swimming vector. Equation (2.9) represents three equations with 12 unknowns. However,  $\mathbf{U}$  in equation (2.8) is arbitrary, and four appropriate choices of  $\mathbf{U}$  yield nine independent equations to solve for all elements of the matrix  $\mathbf{R}$  and vector  $\mathbf{F}_{\text{def}}$ . This is equivalent to the problem of towing the organism with some arbitrary velocity  $\mathbf{U}$  and imposing the external forces and torque that equal the fluid forces and torque calculated by equation (2.7). Once these quantities are found, the swimming vector  $\hat{\mathbf{U}}$  is determined by equation (2.9).

The arbitrary choices of the vector  $\mathbf{U}$  in equation (2.8) are as follows:

- (1)  $\mathbf{U} = \begin{bmatrix} 0 \\ 0 \\ 0 \end{bmatrix}$  gives  $\mathbf{F}_{\text{def}}$
- (2)  $\mathbf{U} = \begin{bmatrix} 1 \\ 0 \\ 0 \end{bmatrix}$  gives  $r_{11}, r_{21} = r_{12}$  and  $r_{31} = r_{31}$
- (3)  $\mathbf{U} = \begin{bmatrix} 0 \\ 1 \\ 0 \end{bmatrix}$  gives  $r_{22}$  and  $r_{32} = r_{23}$
- (4)  $\mathbf{U} = \begin{bmatrix} 0 \\ 0 \\ 1 \end{bmatrix}$  gives  $r_{33}$ .

Finally, once the swimming vector  $\hat{\mathbf{U}}$  is determined, one more simulation is conducted to obtain the pressure and velocity fields, and to extract the forces on the different body parts of the choanoflagellate in the freely swimming form. The above calculations have been performed independently for 12 different positions of the flagellum during the first half of its beat period.

#### 2.1.4. Advection and diffusion of prey

In loricate choanoflagellates, the structure of the lorica is such as to guide the flow through the lorica chamber [3]. In *D. grandis* specifically, the beating flagellum sucks in the water from the lower part of the lorica through the equator and expels it out from the chimney resembling a jet [6]. This arrangement may suggest that the cell is directing the water far away from itself in order to prevent refiltration of once filtered water, a phenomenon which the volume flow rate *per se* does not account for. To test this hypothesis, we assume that prey concentration ( $C$ ) satisfies the advection–diffusion equation [26,27]:

$$\frac{\partial c}{\partial t} + \mathbf{u} \cdot \nabla c = D\nabla^2 c, \quad (2.10)$$

where  $c = C/C_\infty$  is the dimensionless concentration field,  $C_\infty$  the concentration of the prey in the far field, and  $D$  the diffusivity of the prey due to Brownian motion and motility. The collar filter acts as a sink and consumes the prey once it reaches it, essentially leading to a vanishing value of  $c$ . To model this behaviour, we set  $c = 0$  in a thin volume inside the collar filter, in close proximity to the microvilli using a source term that is active in this region [28]. We set  $c = 1$  on the outer boundary where the flow enters the domain. Initially the concentration inside the collar filter volume

is zero and elsewhere  $c = 1$ . Both the advective and the diffusive transport through the filter contribute to the clearance rate:

$$Q_{\text{net}} = - \iint_{S_{\text{filter}}} (c\mathbf{u} - D\nabla c) \cdot \mathbf{n} \, dS. \quad (2.11)$$

The simulations are performed for 40 beat cycles at which time the flow is sufficiently developed and periodicity in the net clearance rate has been obtained.

## 2.2. Observed swimming speed

*Diaphanoeca grandis* (American Type Culture Collection no. 50111) was cultured non-axenically in the dark at 10°C, using B1 medium with a salinity of 32. Organically grown, autoclaved rice grains were added as bacterial substrate [6]. To determine the swimming speed, freely swimming *D. grandis* cells were observed using an Olympus IX-71 inverted microscope equipped with a UPLSA-PO60XO/1.35 oil-immersion objective and a U-ECA magnifying lens. Image sequences were recorded at 100 frames per second and a resolution of 1024 × 800 pixels using a Phantom v210 high-speed camera. Observations were done in a chamber constructed from a 5 mm high polycarbonate ring (diameter approx. 1 cm) mounted with non-hardening silicone between an objective slide and a coverslip.

## 3. Results and discussion

### 3.1. Permeability of the lorica

In this section, we simulate a tethered *D. grandis* and model the lorica as a porous structure with a range of pore sizes between 0.05 and 0.5 μm. Figure 3 depicts the velocity field in the  $xz$ -plane for the two different pore sizes of 0.05 and 0.5 μm averaged over the flagellum beat cycle. A pore size of 0.05 μm practically acts as an impermeable structure (figure 3a). However, as the porosity increases from 0.05 to 0.5 μm, the lorica becomes permeable to the flow (figure 3b), in response to the negative pressure created below the lorica dome (equation (2.5)). Consequently, a portion of the flow reaching the collar filter passes through the lorica dome which results in less flow entering the collar filter through the equator plane. Figure 3c shows the time-averaged flow rate through the equator plane, the collar filter and the lorica dome for a complete beat cycle. The flow through the filter is almost independent of the lorica porosity, and for all cases it is very close to the volume flow rate approximated by the pumping mechanism value of  $Q_V = AW\omega f = 879 \mu\text{m}^3 \text{s}^{-1}$  proposed by Nielsen *et al.* [6] (eqn 5 therein). This is because the flagellum acts nearly as a positive displacement pump in a system of small overall resistance as flow shifts between paths for changing lorica porosity.

Since only the collar filter captures prey, the lorica blocks prey larger than its pore size (i.e. typical bacteria-sized prey) from reaching the filter. Thus, only flow passing the equator plane provides nutrition for the cell, and this decreases as the porosity of the veil increases. This suggests that the lorica costae should be covered either with a fine mesh, which is virtually impermeable to the flow, or with a very coarse mesh, which does not intervene in the prey capture process. An intermediate pore size allows water to pass through while intercepting bacteria-sized prey, consequently impairing the feeding process. In fact, the lorica either contains a fine veil, as compared to the filter spacing, or in some species it appears as an open structure [3]. Nevertheless, even with a medium pore size, more than 80% of the flow goes through the equator

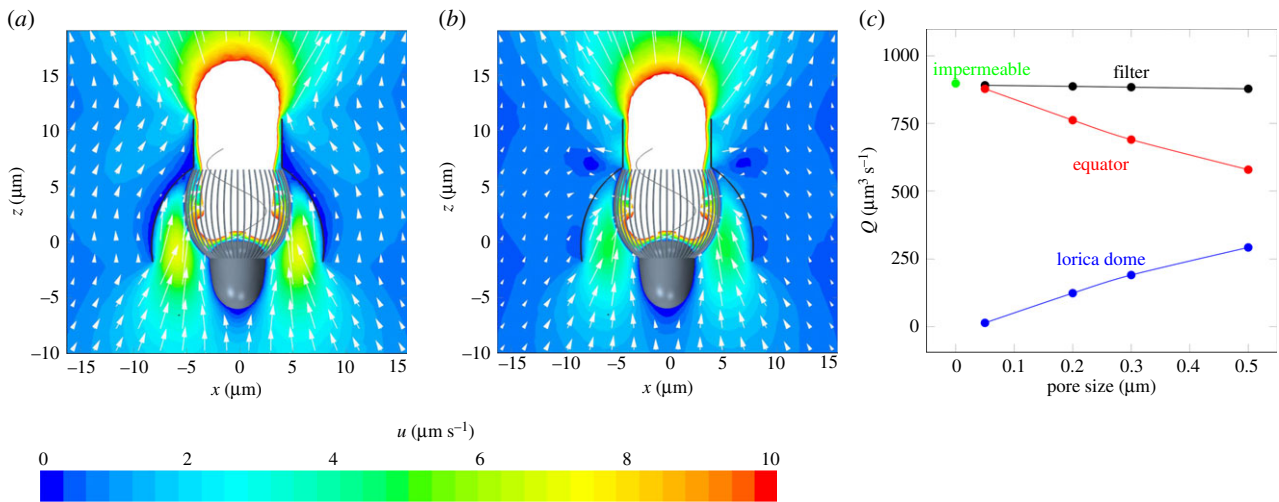


**Figure 3.** Dependence of flow velocities and flow rates on the permeability of the lorica. Velocity field in the  $xz$ -plane for lorica pore sizes of  $0.05 \mu\text{m}$  (a) and  $0.5 \mu\text{m}$  (b) time-averaged over the flagellum beat cycle. For clarity, velocity magnitudes higher than  $10 \mu\text{m s}^{-1}$  are omitted. (c) Mean flow rate through the filter, equator plane and lorica dome for different pore sizes of the lorica. As the pore size increases, the volume flow rate through the equator plane decreases while more flow permeates through the lorica dome which intercepts prey particles larger than its pore size. The flow through the collar filter is independent of the pore size of the lorica and very close to the case of an impermeable lorica. (Online version in colour.)

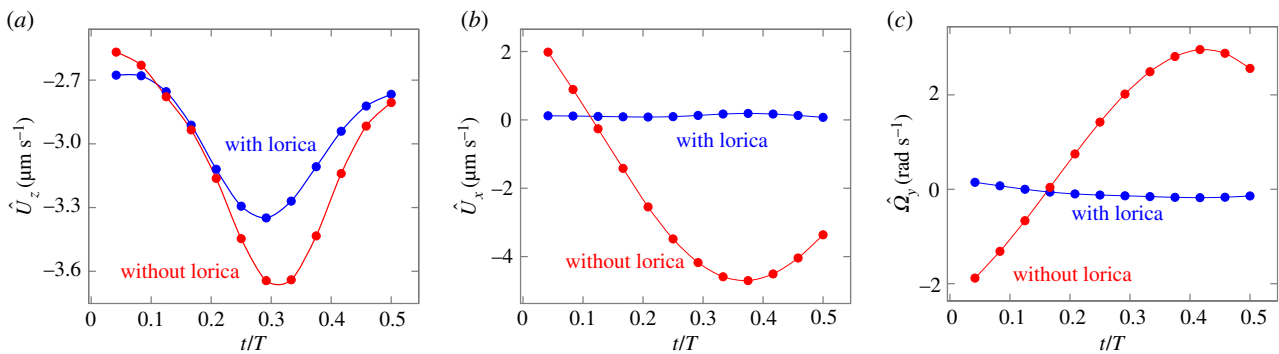


**Figure 4.** Velocity components and rotation rate during one half cycle for *Diaphanoeca grandis* with and without its lorica. The presence of the lorica does not significantly alter the swimming velocity (a), but it dampens significantly the lateral velocity (b) and the rotation rate (c). (Online version in colour.)

plane. Therefore, modelling the lorica as an impermeable structure in the CFD study is an acceptable approximation to the actual structure, and henceforth, employing the previously used CFD model [6], we consider the lorica as an impermeable baffle subject to the no-slip boundary condition.

### 3.2. Swimming motion and power expenditure

Loricata choanoflagellates are generally slow swimmers compared to non-loricata species [3,18]. Figure 4 shows the velocity components and the rotation rate of our modelled freely swimming *D. grandis* with and without its lorica. The forward swimming velocity ( $\hat{U}_z$ ) of *D. grandis* varies slightly during the half cycle with a mean value of  $3.0 \mu\text{m s}^{-1}$  (figure 4a). This is in agreement with experiments where the forward swimming velocity  $U_{\text{exp}} = 2.2 \pm 1.1 \mu\text{m s}^{-1}$  was obtained as the average of six different individuals of *D. grandis*. Forward swimming is the dominant motion of the choanoflagellate and the lateral velocity and rotation are relatively small (figure 4b,c). As a result, *D. grandis* swims smoothly forward along a rather straight line without additional motion (electronic supplementary material, movies S1 and S2). When the lorica is removed, the choanoflagellate appears to remain a slow swimmer with a mean forward swimming velocity of  $3.1 \mu\text{m s}^{-1}$  very close to that of the loricate one. However, in this case, the lateral velocity

components and rotation rate are significant and the cell wiggles from side to side as it swims forward (electronic supplementary material, movie S3). Hence, the lorica appears to stabilize the movement of the cell.

It is striking that the forward swimming velocity of *D. grandis* is almost independent of the presence of a lorica since previously it has been suggested that the lorica slows down the forward motion by imposing significant drag that counteracts the locomotory flagellum force [18]. Table 2 lists the force in the swimming direction on different parts of *D. grandis* with and without its lorica in the freely swimming form, as well as in the case of an externally towed, rigid body with a mean swimming velocity of  $3 \mu\text{m s}^{-1}$ . In the freely swimming *D. grandis* the flagellum force nearly balances the drag on the body and filter, while the drag on the lorica is insignificant.

The reason that the large lorica does not create significant drag is that the flow is driven 'internally' by the beating flagellum. The resulting flow differs markedly from the flow around the towed cell (figure 5). In the latter, the drag force is owing to positive contributions of both the pressure and shear forces [25]. However, in an internal flow, the pressure contribution can counteract the viscous forces depending on the shape of the object and its interaction with other body parts, resulting in a smaller net drag force. This is the case for the lorica, for which the flow is internal. The time-averaged pressure field

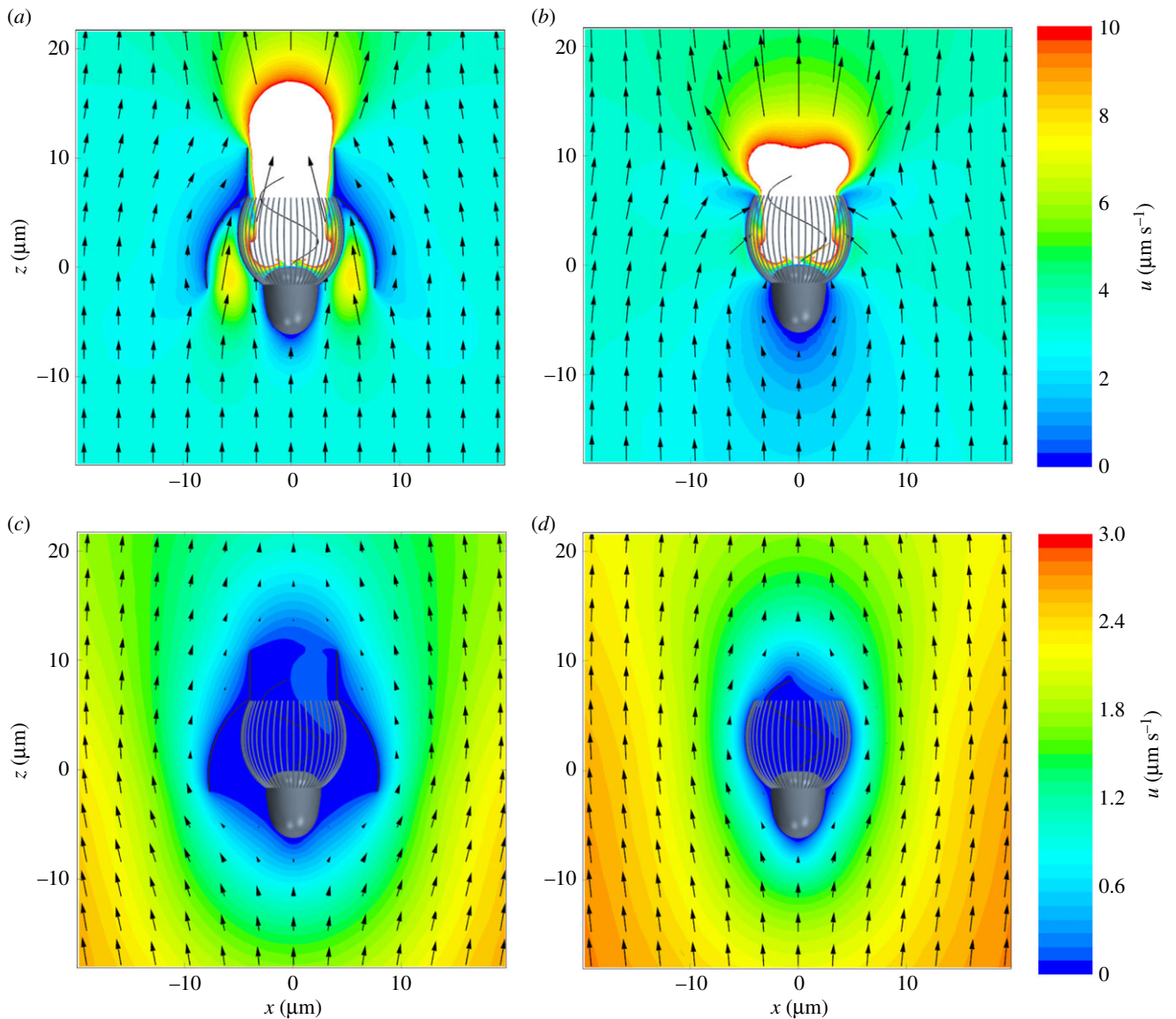


**Figure 5.** Flow fields in the freely swimming and towed choanoflagellates in the frame of reference moving with the cell. (a,b) Velocity field around freely swimming *Diaphanoeca grandis* with and without its lorica averaged over the flagellum beat cycle. (c,d) Velocity field around the towed *D. grandis* with and without its lorica with a velocity of  $3 \mu\text{m s}^{-1}$ . The flow near and through the lorica and the filter is dominated by the beating flagellum. Moreover, when towed, the presence of the lorica reduces the flow velocity over the cell and hence reduces the force on the cell and the collar filter. (Online version in colour.)

**Table 2.** The  $z$ -component of the force on different parts of *Diaphanoeca grandis* with and without its lorica in the freely swimming and towed choanoflagellate with velocity of  $3 \mu\text{m s}^{-1}$  in the swimming direction.

| case            |                | force (pN) |       |        |        |       |
|-----------------|----------------|------------|-------|--------|--------|-------|
|                 |                | flagellum  | cell  | filter | lorica | total |
| freely swimming | with lorica    | -12.091    | 4.343 | 7.169  | 0.580  | 0.001 |
|                 | without lorica | -8.522     | 3.344 | 5.173  | —      | 0.004 |
| towed           | with lorica    | 0.027      | 0.008 | 0.027  | 0.382  | 0.444 |
|                 | without lorica | 0.027      | 0.057 | 0.208  | —      | 0.292 |

in the  $xz$ -plane reveals a low pressure region right below the lorica dome which creates a suction region pulling the lorica down (figure 6). As a result, the pressure force acts in the opposite direction to the flow and counteracts the shear drag such that the net drag on the lorica is comparably small.

When *D. grandis* is towed (or is exposed to an external flow), the drag on the lorica plays a significant role, contributing 86%

to the total drag (table 2). However, the force on the lorica is very small in comparison with the force due to the beating flagellum of the freely swimming organism. In addition, the presence of the lorica significantly decreases the drag force on the filter and the cell by factors of 7.7 and 7.1, respectively. The lorica increases the total external drag force on the choanoflagellate by 52% (table 2).

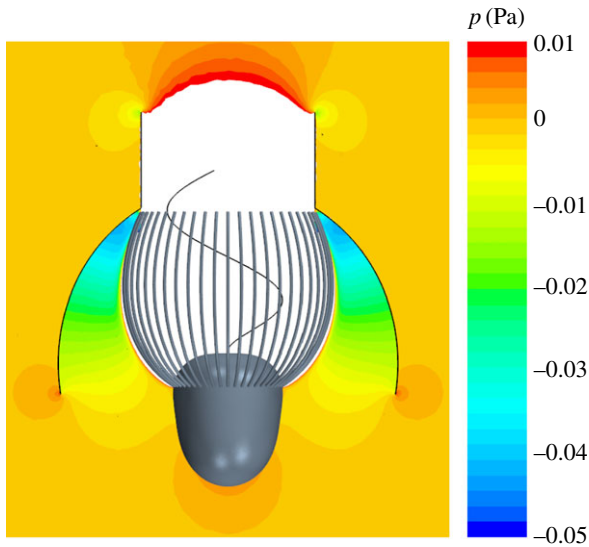


**Figure 6.** The time-averaged pressure field in the  $xz$ -plane around the freely swimming *D. grandis* reveals a low pressure region right below the lorica dome which results in a pressure force in the swimming direction. For clarity, the pressure inside the filter and chimney is not shown. (Online version in colour.)

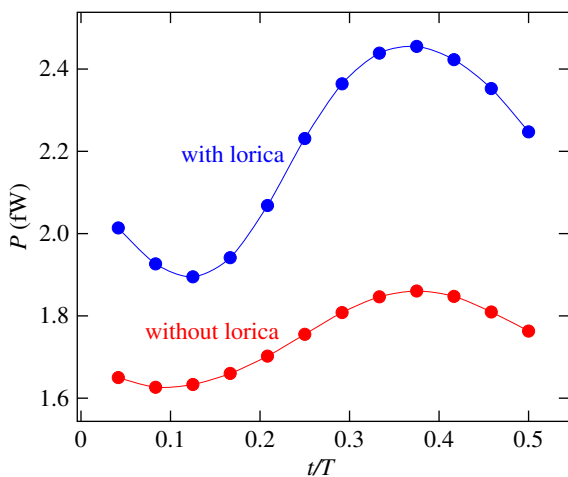


**Figure 7.** Power consumption by the flagellum for *Diaphanoeca grandis* with and without its lorica. The presence of the lorica increases the average required power by approximately 25%, however the power magnitudes are insignificant when compared with the metabolic rate. (Online version in colour.)

Finally, figure 7 shows the mechanical power consumption by the flagellum over a half cycle for *D. grandis* with and without its lorica; the average power consumption is 2.20 and 1.75 fW, respectively. To compare these values to the metabolic budget of the choanoflagellate, we use the size-dependent mass-specific metabolic rate for the flagellate,  $RR = 173 M^{0.17}$  [29], where RR is the specific respiration rate in  $\mu\text{l O}_2 \text{ mg C}^{-1} \text{ h}^{-1}$  and M the body mass of the organism in mgC. As an estimate of the carbon content, we take 10% of the organism mass, resulting in  $9.2 \times 10^{-9}$  mgC. To relate the respiration rate to the metabolic rate, we use a standard oxycalorific value of  $13.8 \text{ J mg O}_2^{-1}$  [30, p. 592] which gives a value of 375 fW, two orders of magnitudes bigger than the power expenditure by the flagellum. Even though the efficiency of conversion is not 100%, the relative cost of beating the flagellum is low, and therefore the additional power consumption with the lorica is insignificant.

**Table 3.** Mean clearance rate  $Q_{\text{net}}$  for different values of diffusivity  $D$ .  $\Delta$  is percentage difference in  $Q_{\text{net}}$  with and without lorica.

| $D$ ( $\mu\text{m}^2 \text{ s}^{-1}$ ) | $Q_{\text{net}}$ ( $\mu\text{m}^3 \text{ s}^{-1}$ ) |                |              |
|--|---|----------------|--------------|
|  | with lorica   | without lorica | $\Delta$ (%) |
| $0.0^a$                                | 902   | 867            | -3.9         |
| 0.0                                    | 900   | 853            | -5.2         |
| 0.4                                    | 904   | 860            | -4.9         |
| 4.0                                    | 920   | 950            | 3.3          |
| 30.0                                   | 1290  | 2150           | 66.7         |

<sup>a</sup>Corresponds to the volume flow rate  $Q$  which is obtained by setting  $c = 1$  in equation (2.11).

### 3.3. Clearance rate

This section presents the effect of the lorica on the clearance rate in the freely swimming choanoflagellate. First we discuss the flow rate through the collar filter, i.e. neglecting the diffusion and depletion of the prey, and then the net clearance rate when advection and diffusion of the prey are considered.

#### 3.3.1. Flow rate through the collar filter

In the absence of prey diffusion, equation (2.11) gives the volume flow rate  $Q$  by setting  $c = 1$  (the case  $D = 0.0$  marked with asterisk in table 3). The lorica has a slight effect on the volume flow rate increasing it only by approximately 5%. This is consistent with the result of §3.1 where the flow passing through the filter is shown to be unaffected by lorica porosity.

Another important aspect is that the slow swimming motion of *D. grandis* does not significantly increase the volume flow rate when compared with the tethered value of  $Q = 898 \mu\text{m}^3 \text{ s}^{-1}$  in the previous study [6]. This is because of a significant resistance by the cell, the filter and the lorica to the swimming, and most of the flow bypasses the collar filter (figure 5c,d).

#### 3.3.2. Advection and diffusion effect

The volume flow rate does not reveal possible effects of flow recirculation and prey diffusivity on feeding. Flow recirculation, i.e. backflow from downstream of the chimney toward the upstream of the lorica, can potentially imply refiltration of already filtered water. To determine a more correct volume cleared for prey, we study the net clearance rate  $Q_{\text{net}}$  of equation (2.11) including advection and diffusion of the prey. Table 3 lists the net clearance rate for different values of prey diffusivity. First we consider only advection of passive prey ( $D = 0.0$ ), i.e. in the limit of infinite Péclet number. This case is suitable to study the possible recirculation of the flow. Here there is only a minor difference (-5.2%) in the net clearance rate of *D. grandis* with and without its lorica. The function of the lorica is thus not to prevent recirculation.

The case  $D = 0.4 \mu\text{m}^2 \text{ s}^{-1}$  in table 3 corresponds to the effective diffusivity due to the Brownian motion of a typical spherical prey of  $0.5 \mu\text{m}$  in diameter at  $16^\circ\text{C}$ . In this regime, the advective transport is dominant, and the difference in the clearance rate is still small. Although the chimney in *D. grandis* directs the flow far from the choanoflagellate resembling a jet, there is still no sign of recirculation even after the lorica is removed (figure 8a). However, as we increase the diffusivity

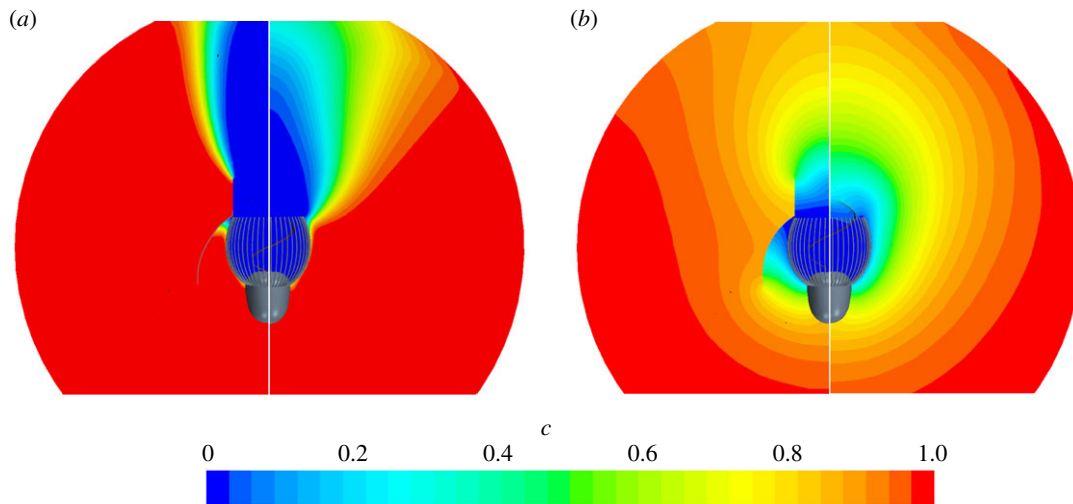


**Figure 8.** Prey concentration  $c$  in the  $xz$ -plane around the freely swimming *Diaphanoeca grandis*. (a)  $D = 0.4 \mu\text{m}^2 \text{s}^{-1}$  which corresponds to the effective diffusivity of typical passive prey due to Brownian motion. (b)  $D = 30 \mu\text{m}^2 \text{s}^{-1}$  which corresponds to the effective diffusivity of typical motile prey. For each case, the left and right half of the plot shows the result with and without its lorica, respectively. At small diffusivity (high Pe), advection is the dominating transport factor while at higher diffusivity (low Pe), diffusion becomes dominant. In this case, the lorica would act as an insulation to prey diffusion towards the filter, thus reducing the net clearance rate as compared to that of the non-loricated case. (Online version in colour.)

$D$ , i.e. smaller Péclet number, the clearance rate becomes dominated by the diffusion mechanism. At  $D = 30 \mu\text{m}^2 \text{s}^{-1}$ , which is the effective diffusivity of a typical motile prey with swimming speed  $44 \mu\text{m} \text{s}^{-1}$  and run time  $0.04 \text{s}$  [31], the net clearance rate of the non-loricated choanoflagellate surpasses the loricated one by 67% (table 3). In a pure diffusive transport regime, the flux through a spherical sink in an infinite domain is  $Q_{\text{diff}} = 4\pi DR_{\text{sink}}$ , where  $R_{\text{sink}}$  is the radius of the sink [32]. Employing a mean filter radius of  $R_f = 4.3 \mu\text{m}$  and a diffusivity of  $D = 30 \mu\text{m}^2 \text{s}^{-1}$ , for the case without the lorica we find  $Q_{\text{diff}} = 1620 \mu\text{m}^3 \text{s}^{-1}$  comparable with the total clearance rate indicating the complete dominance of diffusive transport when prey motility is considered. In such a diffusion-dominated regime, the lorica suppresses the prey transfer toward the filter (figure 8b). This suggests that loricated choanoflagellates are inefficient feeders on motile bacteria.

### 3.4. Prey retention

Thus far, our results on clearance rates for different scenarios and energy expenditure reveal no significant advantage of the lorica, but rather the opposite for motile prey. However, the clearance rate estimated above assumes that all encountered prey are captured. One should also consider the efficiency of prey capture, that is the ratio of the number of prey particles captured to those encountered. Filter feeding consists of three successive steps: prey encounter, retention and handling [33]. Once the prey is in contact with the microvilli during the encounter process, the cell must retain and transfer it down to the base of the collar toward the cell where it is phagocytosed. This process may take several seconds [20], and in the choanoflagellate *Salpingoeca rosetta*, Dayel *et al.* [34] report that the movement of bacteria prey to the base and engulfing takes on average 12.5 s and 20 s, respectively. Given that the flagellum beat period in choanoflagellates is a fraction of a second, the prey experiences hundreds of beat cycles as it is being moved along the collar, with a potential to be lost before being engulfed. We speculate that the lorica increases the efficiency of prey capture by three mechanisms.

Firstly, without the lorica, the cell and specifically the microvilli exhibit intense movements from side to side, which possibly hinders prey retention and transportation down to the base of the collar. However in the loricated cells, the lorica stabilizes cell motion by reducing the lateral motion of the cell and microvilli which could reduce the risk of prey escape. Being thecate or part of a colony could have a similar effect where the cells attach to a substrate or stick together via filopodia and intercellular bridges [35–37]. Attachment or colony formation stabilizes the individual cell and the collar motion, potentially increasing the retention efficiency. This could also be the reason why the flagella beat is not synchronized in colonies [38,39], as the lateral force and torque from neighbouring cells would stack rather than cancel out.

Secondly, while the flagellum is beating, in some areas at the distal part of the microvilli, the flow direction is outward from the collar. This phenomenon is observed in both loricated and non-loricated cells, but it is much more intense in the latter. Figure 9 depicts snapshots of the velocity field between the microvilli in the  $xz$ -plane. Without the lorica, the velocity in the upper part of the collar is outward and bigger in magnitude than for the loricated one. Including the lorica mitigates this effect not only by lowering the velocity magnitude, but also by slight downward deflection of the flow. This may increase the likelihood of prey retention on the collar. For the cell to retain a passive prey that encounters the outer surface of the microvilli, the adhesive force by the collar must equal or exceed the local fluid forces resisting the adhesion [33]. For a given adhesive force, the smaller the local fluid forces on the particle, the bigger the likelihood of the bacteria retention on the collar. The lorica reduces velocities on the distal part of the filter, and thus could improve prey retention. Poor particle retention and loss of bacteria from the distal part of the collar has been observed in some species of non-loricated choanoflagellates such as *Salpingoeca amphoridium* [40] and *S. rosetta* single cells and colonies [34]. Another remedy to this problem would be to have the prey capture zone mostly on the lower part of the microvilli where there is no outflow; the veil in the loricated choanoflagellate *Didymoeca costata* guides the



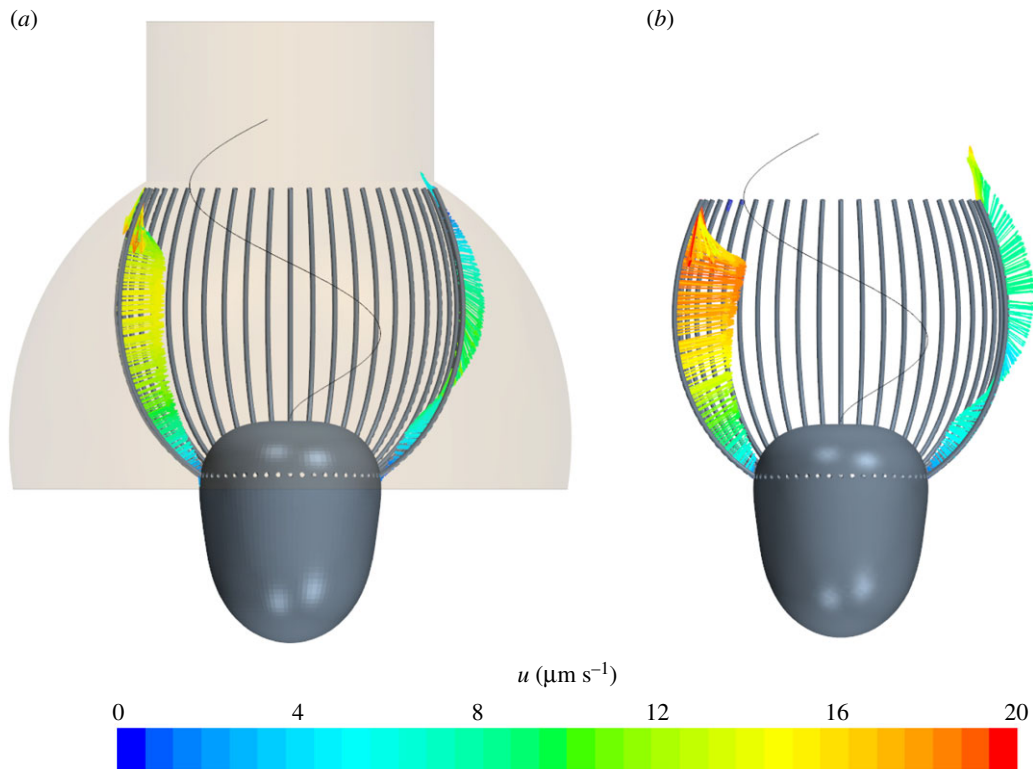


**Figure 9.** Snapshot of the velocity field between the microvilli in the flagellar beat plane ( $xz$ -plane) of *Diaphanoeca grandis* with (a) and without (b) its lorica. The lorica mitigates the outward flow from the distal part of the microvilli, potentially increasing the chance of retaining the prey on the collar. (Online version in colour.)

inflow directly toward the collar base [3] where the prey is immediately captured and ingested.

Thirdly, the lorica chamber, especially in species with a veil on the inner surface of the lorica such as *D. grandis*, *D. costata* and *Crinolina aperta*, is similar to a trap; even if the prey escapes from the collar, the lorica veil does not allow it to go beyond reach and it is more likely for the choanoflagellate to recapture its prey.

## 4. Conclusion

In this study, using detailed CFD simulations, we explore the hydrodynamic function of the lorica in the standard tectiform loricate choanoflagellate *D. grandis*. Our results provide no support for the several previous hypotheses regarding the effects of the choanoflagellate lorica. Rather, our simulations suggest that the main function of the lorica is to

enhance the capture efficiency, but this happens at the cost of lower encounter rate with motile prey. We note that our study concerns mainly hydrodynamic effects of the lorica. There could well be other effects of the lorica, including e.g. protection against predators.

**Data accessibility.** Data for the model morphology and numerical modelling are described in this paper and in the supplementary material.

**Authors' contributions.** All authors designed the research and wrote the paper. S.S.A., A.A., J.D., P.S.L. and J.H.W. developed the model and the mathematical framework for the CFD simulations. L.T.N. and T.K. provided biological advice on the model and interpreting the results. L.T.N. did the experiment. S.S.A. performed the simulations.

**Competing interests.** The authors declare no competing interests.

**Funding.** We gratefully acknowledge funding from the Villum Foundation for S.S.A. and J.H.W. through research grant no. 9278 and for A.A., J.D., L.T.N. and T.K. through the Centre for Ocean Life. T.K., A.A. and L.T.N. were further supported by The Independent Research Fund Denmark (grant no. 7014-00033B).

## References

- Fenchel T. 1984 Suspended marine bacteria as a food source. In *Flows of energy and materials in marine ecosystems*, pp. 301–315. Berlin, Germany: Springer.
- Fenchel T. 1986 Protozoan filter feeding. *Prog. Protistol.* **1**, 65–113.
- Leadbeater BSC. 2015 *The choanoflagellates: evolution, biology and ecology*, 1st edn. Cambridge, UK: Cambridge University Press.
- Mah JL, Christensen-Dalsgaard KK, Leys SP. 2014 Choanoflagellate and choanocyte collar-flagellar systems and the assumption of homology. *Evol. Dev.* **16**, 25–37. (doi:10.1111/ede.v16.1)
- Maldonado M. 2004 Choanoflagellates, choanocytes, and animal multicellularity. *Invert. Biol.* **123**, 1–22. (doi:10.1111/ivb.2004.123.issue-1)
- Nielsen LT, Asadzadeh SS, Dölger J, Walther JH, Kiørboe T, Andersen A. 2017 Hydrodynamics of microbial filter feeding. *Proc. Natl Acad. Sci. USA* **114**, 9373–9378. (doi:10.1073/pnas.1708873114)
- Purcell EM. 1977 Life at low Reynolds number. *Am. J. Phys.* **45**, 3–11. (doi:10.1119/1.10903)
- Lauga E, Powers TR. 2009 The hydrodynamics of swimming microorganisms. *Rep. Prog. Phys.* **72**, 096601. (doi:10.1088/0034-4885/72/9/096601)
- Kiørboe T. 2011 How zooplankton feed: mechanisms, traits and trade-offs. *Biol. Rev.* **86**, 311–339. (doi:10.1111/brv.2011.86.issue-2)
- Fjordingstad EJ. 1961 The ultrastructure of choanocyte collars in *Spongilla lacustris* (L.). *Z. Zellforsch.* **53**, 645–657. (doi:10.1007/BF00339512)
- Mehl D, Reiswig HM. 1991 The presence of flagellar vanes in choanomers of Porifera and their possible phylogenetic implications. *J. Zoo. Syst. Evol. Res.* **29**, 312–319. (doi:10.1111/j.1439-0469.1991.tb00676.x)

12. Weissenfels N. 1992 The filtration apparatus for food collection in freshwater sponges (Porifera, Spongillidae). *Zoomorphology* **112**, 51–55. (doi:10.1007/BF01632994)
13. Leadbeater BSC. 2006 The mystery of the flagellar vane in choanoflagellates. *Nova Hedwigia Beiheft* **130**, 213–223.
14. Asadzadeh SS, Larsen PS, Riisgård HU, Walther JH. In press. Hydrodynamics of the leucon sponge pump. *J. R. Soc. Interface*.
15. Larsen PS, Riisgård HU. 1994 The sponge pump. *J. Theor. Biol.* **168**, 53–63. (doi:10.1006/jtbi.1994.1087)
16. Leys SP, Yahel G, Reidenbach A, Tunnicliffe V, Shavit U, Reiswig H. 2011 The sponge pump: the role of current induced flow in the design of the sponge body plan. *PLoS ONE* **6**, e27787. (doi:10.1371/journal.pone.0027787)
17. Ludeman DA, Reidenbach MA, Leys SP. 2017 The energetic cost of filtration by demosponges and their behavioural response to ambient currents. *J. Exp. Biol.* **220**, 995–1007. (doi:10.1242/jeb.146076)
18. Andersen P. 1988 Functional biology of the choanoflagellate *Diaphanoeca grandis* Ellis. *Mar. Microb. Food Webs* **3**, 35–50.
19. Walsby AE, Xypolyta A. 1977 The form resistance of chitan fibres attached to the cells of *Thalassiosira fluviatilis* Hustedt. *Br. Phycol. J.* **12**, 215–223. (doi:10.1080/00071617700650231)
20. Pettitt ME, Orme BAA, Blake JR, Leadbeater BSC. 2002 The hydrodynamics of filter feeding in choanoflagellates. *Eur. J. Protist.* **38**, 313–332. (doi:10.1078/0932-4739-00854)
21. Higdon JLL. 1979 A hydrodynamic analysis of flagellar propulsion. *J. Fluid Mech.* **90**, 685–711. (doi:10.1017/S0022112079002482)
22. Sleight MA. 1991 Mechanisms of flagellar propulsion. *Protoplasma* **164**, 45–53. (doi:10.1007/BF01320814)
23. Batchelor GK. 1967 *An introduction to fluid dynamics*, 1st edn. Cambridge, UK: Cambridge University Press.
24. Silvester NR. 1983 Some hydrodynamic aspects of filter feeding with rectangular-mesh nets. *J. Theor. Biol.* **103**, 265–286. (doi:10.1016/0022-5193(83)90028-0)
25. Happel J, Brenner H. 1983 *Low Reynolds number hydrodynamics*, 2nd edn. Dordrecht, The Netherlands: Kluwer Academic Publishers.
26. Michelin S, Lauga E. 2011 Optimal feeding is optimal swimming for all Péclet numbers. *Phys. Fluids* **23**, 101901. (doi:10.1063/1.3642645)
27. Kirkegaard JB, Goldstein RE. 2016 Filter-feeding, near-field flows, and the morphologies of colonial choanoflagellates. *Phys. Rev. E* **94**, 052401. (doi:10.1103/PhysRevE.94.052401)
28. Patankar SV. 1980 *Numerical heat transfer and fluid flow*. Washington, DC: Hemisphere.
29. Kiørboe T, Hirst AG. 2014 Shifts in mass scaling of respiration, feeding, and growth rates across life-form transitions in marine pelagic organisms. *Am. Nat.* **183**, E118–E130. (doi:10.1086/675241)
30. Gordon SG. 1972 *Animal physiology: principles and adaptations*, 2nd edn. New York, NY: Macmillan Publishing Co.
31. Dölger J, Nielsen LT, Kiørboe T, Andersen A. 2017 Swimming and feeding of mixotrophic biflagellates. *Sci. Rep.* **7**, 39892. (doi:10.1038/srep39892)
32. Berg HC. 1993 *Random walks in biology*. Princeton, NY: Princeton University Press.
33. Shimeta J, Koehl MAR. 1997 Mechanisms of particle selection by tentaculate suspension feeders during encounter, retention, and handling. *J. Exp. Mar. Biol. Ecol.* **209**, 47–73. (doi:10.1016/S0022-0981(96)02684-6)
34. Dayel M, King N. 2014 Prey capture and phagocytosis in the choanoflagellate *Salpingoeca rosetta*. *PLoS ONE* **9**, e95577. (doi:10.1371/journal.pone.0095577)
35. Dayel M, Alegado R, Fairclough S, Levin T, Nichols S, McDonald K, King N. 2011 Cell differentiation and morphogenesis in the colony-forming choanoflagellate *Salpingoeca rosetta*. *Dev. Biol.* **357**, 73–82. (doi:10.1016/j.ydbio.2011.06.003)
36. Sebé-Pedrós A, Burkhardt P, Sánchez-Pons N, Fairclough SR, Franz Lang B, King N, Ruiz-Trillo I. 2013 Insights into the origin of metazoan filopodia and microvilli. *Mol. Biol. Evol.* **30**, 2013–2023. (doi:10.1093/molbev/mst110)
37. Hoffmeyer TT, Burkhardt P. 2016 Choanoflagellate models—*Monosiga brevicollis* and *Salpingoeca rosetta*. *Curr. Opin. Struct. Biol.* **39**, 42–47. (doi:10.1016/j.gde.2016.05.016)
38. Kirkegaard JB, Marron AO, Goldstein RE. 2016 Motility of colonial choanoflagellates and the statistics of aggregate random walkers. *Phys. Rev. Lett.* **116**, 038102. (doi:10.1103/PhysRevLett.116.038102)
39. Roper M, Dayel MJ, Pepper RE, Koehl MAR. 2013 Cooperatively generated stresslet flows supply fresh fluid to multicellular choanoflagellate colonies. *Phys. Rev. Lett.* **110**, 228104. (doi:10.1103/PhysRevLett.110.228104)
40. Pettitt ME. 2001 Prey capture and ingestion in choanoflagellates. PhD thesis, University of Birmingham.